

# Major element stream water chemistry, compiled $^{10}\text{Be}$ erosion rates, and analyses of weathering across an erosion-rate gradient in southern Taiwan

(<https://doi.org/10.5880/GFZ.4.6.2021.001>)

---

Aaron Bufe<sup>1</sup>, Niels Hovius<sup>1,2</sup>, Robert Emberson<sup>3</sup>, Jeremy K. Caves Rugenstein<sup>4</sup>, Albert Galy<sup>5</sup>, Hima J. Hassenruck-Gudipati<sup>6</sup>, and Jui-Ming Chang<sup>7</sup>.

1. *GFZ German Research Centre for Geosciences, Telegrafenberg, 14473 Potsdam, Germany.*
2. *Institute of Geosciences, University of Potsdam, Karl Liebknecht Strasse 24-25, 14476 Potsdam, Germany.*
3. *NASA Goddard Space Flight Center, Greenbelt, MD 20771, USA.*
4. *Max Planck Institute for Meteorology, Bundesstraße 53 20146 Hamburg, Germany.*
5. *Centre de Recherches Pétrographiques et Géochimiques, UMR7358, CNRS, Université de Lorraine, 54500 Nancy, France.*
6. *Jackson School of Geosciences, University of Texas at Austin, Austin, TX 78712, USA.*
7. *Department of Geosciences, National Taiwan University, 10617 Taipei, Taiwan*

## 1. Licence

Creative Commons Attribution 4.0 International License (CC BY 4.0)



## 2. Citation

**When using the data please cite:**

Bufe, A., Hovius, N., Emberson, R., Caves Rugenstein, J.K., Galy, A., Hassenruck-Gudipati, H., Chang, J.-M. (2021): Major element stream water chemistry, compiled  $^{10}\text{Be}$  erosion rates, and analyses of weathering across an erosion-rate gradient in southern Taiwan. GFZ Data Services.  
<https://doi.org/10.5880/GFZ.4.6.2021.001>

**The data are supplementary material to:**

Bufe, A., Hovius, N., Emberson, R., Rugenstein, J. K. C., Galy, A., Hassenruck-Gudipati, H. J., & Chang, J.-M. (2021). Co-variation of silicate, carbonate and sulfide weathering drives  $\text{CO}_2$  release with erosion. *Nature Geoscience*, 14(4), 211–216. <https://doi.org/10.1038/s41561-021-00714-3>

## Table of contents

|   |    |
|---|----|
| 1. Licence .....  | 1  |
| 2. Citation .....   | 1  |
| Table of contents .....                                       | 2  |
| 3. Data Description .....                                     | 2  |
| 3.1. Sampling method .....                                    | 2  |
| 3.2. Analytical procedure: .....                              | 3  |
| 3.3. Data processing .....                                    | 3  |
| Notations and constants .....                                 | 3  |
| Erosion rate – ksn scaling .....                              | 3  |
| Unmixing major contributions to the cation solute budget..... | 4  |
| Estimate of sulphuric acid contribution to weathering.....    | 5  |
| Corrections for secondary precipitation of calcite .....      | 5  |
| CO <sub>2</sub> budget from weathering reactions .....        | 6  |
| Estimate of pH change due to addition of sulphuric acid ..... | 8  |
| 4. File description .....                                     | 10 |
| 5. Acknowledgement.....                                       | 11 |
| 6. References .....   | 11 |

## 3. Data Description

This dataset was used to analyse the link between chemical weathering and erosion rates across the southern tip of Taiwan. The weathering of silicate minerals is a key component of Earth's long-term carbon cycle, and it stabilises Earth's climate by sequestering carbon dioxide (CO<sub>2</sub>) from the atmosphere – thereby balancing CO<sub>2</sub>-emissions from the mantle. Conversely, the weathering of accessory carbonate and sulphides acts as a CO<sub>2</sub> source. Chemical weathering is fundamentally dependent on the exposure of fresh minerals by erosion. With these data we investigated the link between the exposure of rocks by erosion and the chemical weathering of silicates, carbonates, and sulphides across a landscape with a significant erosion-rate gradient and comparatively little variation in runoff and lithology

This dataset includes new major element chemistry and water isotopes of river waters collected from across the southern tip of Taiwan as well as associated topographic and lithologic data (tab 1 in the excel table). Moreover, the data include a compilation of published <sup>10</sup>Be-derived erosion rates from a subset of the sampled rivers (tab 2 in the excel file) and available major element chemistry from hotspots in the region (tab 3 in the excel file). Using a mixing model, we derived the cation contributions from silicate and carbonate weathering as well as from hotspots and cyclic sources. Further, we estimated the erosion rates for each sample from the compiled <sup>10</sup>Be data and the steepness of river channels, and we estimated saturation and pH in the weathering zone.

### 3.1. Sampling method

The following text is a shortened excerpt from the methods section of Bufe et al. (2021).

During two field seasons in February-March 2015 and May-June 2017, we collected 119 water samples across southern Taiwan for chemical analysis in 1-liter HDPE bottles from river banks with access to the main flow. All samples were filtered the evening after sampling into a set of smaller HDPE bottles (for anion and cation measurements as well as water isotope analyses) using 0.22 µm Merck Express Plus Membrane filters. We rinsed each bottle with filtered water before filling, and we acidified all bottles for cation analyses with concentrated ultrapure nitric acid (HNO<sub>3</sub>). We measured pH and

temperature of the river in the field at the sample location using a WTW Multi 3430 Multimeter and a WTW SensoLyt 900 pH probe. Electrical conductivity and dissolved oxygen content of the water were measured with a WTW TetraCon 925 and a WTW FDO 925 probe respectively.

### 3.2. Analytical procedure:

The following text is a shortened excerpt from the methods section of Bufe et al. (2021).

After dilution with a Cs-spiked solution, cations ( $Ba^{2+}$ ,  $Ca^{2+}$ ,  $Fe^{2+}$ ,  $K^+$ ,  $Li^+$ ,  $Mg^{2+}$ ,  $Mn^{2+}$ ,  $Na^+$ , and  $Sr^{2+}$ ) and dissolved silica were measured on a Varian 720 ICP-OES at the German Research Centre for Geosciences (GFZ). Every 10 samples a quality control sample, mixed at the GFZ, was measured to monitor machine drift. All accepted runs had a drift of <5%. We measured external river water standards SLRS-5 or SLRS-6 and USGS-T187 and M212 for quality control. The measurements were calibrated using a set of 11 in-house standards, and any standards that did not fall within 10% of a linear fit through all standards were discarded. We only used measurements within the range of accepted standards, and estimated the uncertainty in the cation analysis from the maximum deviation of the calibration standards from the calibration line. We measured major anions, ( $Cl^-$ ,  $NO_3^-$ ,  $SO_4^{2-}$ ), on a Dionex ICS-1100 chromatograph using a six-point linear calibration and USGS 206 and 212 standards for quality-control. For samples from 2017, we also measured concentrations of fluorine ( $F^-$ ). Uncertainty estimates were based on the standard deviation from three repeat measurements. Finally, we measured water isotopes of stream samples on a Picarro 2140i at the GFZ. Bicarbonate concentrations ( $HCO_3^-$ ) were estimated by charge balance, which assumes that the contribution of bicarbonate from organic sources is negligible (Text S4). Uncertainties were propagated from the analytical uncertainties of the measured concentrations.

### 3.3. Data processing

The following text is a shortened excerpt from the methods section of Bufe et al. (2021).

#### Notations and constants

We use the following notations:  $[i]$ , is the concentration of ion  $i$ ,  $v_i$  is the valence of ion  $i$ ,  $[i]^{eq} = v_i[i]$  is the charge equivalent concentration of ion  $i$ ,  $\gamma_i$  is the activity coefficient of ion  $i$ , and  $a_i$  is the activity of ion  $i$  with  $a_i = \gamma_i[i]$ . Subscripts *carb*, *sil*, and *sulf*, denote quantities calculated for the ions derived from carbonate, silicate, and sulphide weathering, and the subscripts *hs*, *cy*, *sc*, and *tot* refer to contributions from hot springs, cyclic sources, silicate and carbonate weathering, and the total solute budget. We use the equilibrium constants and standard enthalpies as specified in Table 1.

#### Erosion rate – ksn scaling

We used a regression between existing cosmogenic nuclide erosion rate data (Chen et al., 2020; Fellin et al., 2017) and the catchment-averaged steepness indices to predict catchment-averaged erosion rates for each of our water samples. First, we calculated mean steepness indices upstream of each cosmogenic nuclide sample and upstream of each water sample using TopoToolbox V2.2 (Schwanghart & Scherler, 2014). Cosmogenic nuclide concentrations in southern Taiwan decrease northward, and concentrations in repeat samples collected in 2006 and 2015/16 generally agree (Chen et al., 2020; Fellin et al., 2017). We used a regression through the catchment-averaged normalized steepness and catchment-averaged erosion rates to predict, from the steepness index, a catchment averaged erosion rate for each of the water samples collected in this study. Uncertainties in erosion-rates were estimated from the confidence band of the regression. We excluded all data from 2012 from the analysis, because of the potential impact of Typhoon Morakot on the data (Chen et al., 2020).

### Unmixing major contributions to the cation solute budget

In our analysis, we only considered the major cations  $Ca^{2+}$ ,  $Mg^{2+}$ ,  $K^+$ , and  $Na^+$  and contributions from carbonates, silicates, cyclic water, and hotsprings to the cation budget. The concentrations of cations derived from carbonate weathering,  $[Cat]_{carb}$ , silicate weathering,  $[Cat]_{sil}$ , the sum of silicate and carbonate weathering  $[Cat]_{wtot}$ , cyclic contributions  $[Cat]_{cy}$ , and hotsprings  $[Cat]_{hs}$ , are:

$$[Cat]_{carb} = \sum_i [i]_{carb}; [Cat]_{sil} = \sum_i [i]_{sil}; [Cat]_{wtot} = [Cat]_{sil} + [Cat]_{carb}; [Cat]_{cy} = \sum_i [i]_{cy}; [Cat]_{hs} = \sum_i [i]_{hs}; \quad (1).$$

We define corresponding charge equivalent concentrations,  $[Cat]^{eq}$ , as:

$$[Cat]_{carb}^{eq} = \sum_i v_i [i]_{carb}; [Cat]_{sil}^{eq} = \sum_i v_i [i]_{sil}; [Cat]_{wtot}^{eq} = [Cat]_{sil}^{eq} + [Cat]_{carb}^{eq}; [Cat]_{cy}^{eq} = \sum_i v_i [i]_{cy}; [Cat]_{hs}^{eq} = \sum_i v_i [i]_{hs}; \quad (2).$$

The fraction of cation charge related to carbonate weathering,  $f_{carb}$ , and the fraction of cation charge balanced by sulphate,  $f_{sulf}$ , are defined as:

$$f_{carb} = \frac{[Cat]_{carb}^{eq}}{[Cat]_{wtot}^{eq}}; f_{sulf} = \frac{[SO_4^{2-}]_{sulf}^{eq}}{[Cat]_{wtot}^{eq}} \quad (3).$$

We used an inverse approach to estimate the contribution of carbonate and silicate minerals to the dissolved solids. Following previous authors (Burke et al., 2018; Emberson et al., 2018; Gaillardet et al., 1999; Moon et al., 2014; West et al., 2005), this estimate was based on modelling the relative concentrations of three major soluble cations,  $Na^+$ ,  $Ca^{2+}$ , and  $Mg^{2+}$  as a mix of a silicate and a carbonate endmember (Table 2). In addition, here we include the concentration of  $Cl^-$ , to allow correction of the cyclic and hotspring contribution (Table 2). Based on these endmembers, we solved the following equations using the linear least squares solver lsqin in MATLAB:

$$\left[ \frac{Na^+}{Ca^{2+}} \right]_m = \alpha_{Ca,sil} \left[ \frac{Na^+}{Ca^{2+}} \right]_{sil} + \alpha_{Ca,carb} \left[ \frac{Na^+}{Ca^{2+}} \right]_{carb} + \alpha_{Ca,cy} \left[ \frac{Na^+}{Ca^{2+}} \right]_{cy} + \alpha_{Ca,hs} \left[ \frac{Na^+}{Ca^{2+}} \right]_{hs} \quad (4),$$

$$\left[ \frac{Mg^{2+}}{Ca^{2+}} \right]_m = \alpha_{Ca,sil} \left[ \frac{Mg^{2+}}{Ca^{2+}} \right]_{sil} + \alpha_{Ca,carb} \left[ \frac{Mg^{2+}}{Ca^{2+}} \right]_{carb} + \alpha_{Ca,cy} \left[ \frac{Mg^{2+}}{Ca^{2+}} \right]_{cy} + \alpha_{Ca,hs} \left[ \frac{Mg^{2+}}{Ca^{2+}} \right]_{hs} \quad (5),$$

$$\left[ \frac{Cl^-}{Ca^{2+}} \right]_m = \alpha_{Ca,sil} \left[ \frac{Cl^-}{Ca^{2+}} \right]_{sil} + \alpha_{Ca,carb} \left[ \frac{Cl^-}{Ca^{2+}} \right]_{carb} + \alpha_{Ca,cy} \left[ \frac{Cl^-}{Ca^{2+}} \right]_{cy} + \alpha_{Ca,hs} \left[ \frac{Cl^-}{Ca^{2+}} \right]_{hs} \quad (6),$$

under the conditions that:

$$\alpha_{Ca,sil} + \alpha_{Ca,carb} + \alpha_{Ca,cy} + \alpha_{Ca,hs} = 1 \quad (7),$$

and

$$0 \leq \alpha_{Ca,sil} \leq 1; 0 \leq \alpha_{Ca,carb} \leq 1; 0 \leq \alpha_{Ca,cy} \leq 1; 0 \leq \alpha_{Ca,hs} \leq 1 \quad (8),$$

where  $\alpha_{Ca,sil}$ ,  $\alpha_{Ca,carb}$ ,  $\alpha_{Ca,cy}$  and  $\alpha_{Ca,hs}$  are the fractions of calcium sourced from silicate weathering, carbonate weathering, cyclic input, and hotspring input respectively. Following previous authors (Moon et al, 2014), we estimated pairs of “best fit” endmembers for each sample with 10,000 Monte Carlo runs. In each run, we randomly picked a set of two endmembers from normal distributions defined by the mean and the standard deviation of the local endmember estimates (Table 2). For each sample, we then obtained an individual endmember estimate from the mean and standard deviation of all Monte Carlo runs that were weighted by the inverse chi-squared misfit between model and data of each run. One sample with an anomalously high ratio of  $\left[\frac{Mg^{2+}}{Ca^{2+}}\right]$  was discarded from the inversion because it does not fall within the bounds of the silicate-carbonate-hotspring-cyclic endmember.

#### Estimate of sulphuric acid contribution to weathering

The contribution of weathering by sulphuric acid was estimated from the total sulphate concentrations corrected for cyclic and hotspring inputs:

$$[SO_4^{2-}]_{sulf} = [SO_4^{2-}]_m - [SO_4^{2-}]_{cy} - [SO_4^{2-}]_{hs} \quad (9),$$

with

$$[SO_4^{2-}]_{cy} = \alpha_{Ca,cy} \left[ \frac{SO_4^{2-}}{Ca^{2+}} \right]_{cy} ; \quad [SO_4^{2-}]_{hs} = \alpha_{Ca,hs} \left[ \frac{SO_4^{2-}}{Ca^{2+}} \right]_{hs} \quad (10).$$

This calculation assumes negligible anthropogenic and evaporite inputs of sulphate to Taiwanese rivers and an absence of major sulphate sinks (Text S4).

#### Corrections for secondary precipitation of calcite

The enrichment of waters in  $Sr^{2+}$  relative to  $Ca^{2+}$  and  $Na^+$  can be used as an indicator for secondary precipitation of calcite (Bickle et al., 2015; Emberson et al., 2018). Assuming that all measured Sr is contributed from chemical weathering, solutes from a mixed silicate and carbonate source that have not experienced re-precipitation of calcite should fall on a mixing line between a pure calcite endmember at  $\left[\frac{Na^+}{Ca^{2+}}\right]$  close to zero and  $1000 \left[\frac{Sr^{2+}}{Ca^{2+}}\right] = 1 - 2$ , and a silicate endmember with both a higher  $\left[\frac{Na^+}{Ca^{2+}}\right]$  and a higher  $\left[\frac{Sr^{2+}}{Ca^{2+}}\right]$  ratio (Emberson et al., 2018). We assumed that the published elemental analyses of suspended sediments sampled in the Chenyoulan river (Emberson et al., 2018) approximate the endmember mixing line between silicates and carbonates, and we found the best fit line through these data that is described by:

$$\frac{1000 \times [Sr]}{[Ca]} = a + b \frac{[Na]}{[Ca]} \quad (11),$$

where  $a$  and  $b$  are the parameter of the linear fit. With precipitation of calcium, the Sr/Ca ratio increases according to:

$$\frac{[Sr]_f}{[Ca]_f} = \frac{[Sr]_0}{[Ca]_0} \beta^{(kd-1)} \quad (12),$$

where subscripts 0 and  $f$  denote the initial and final concentrations respectively,  $kd$  is the partition coefficient for Sr into abiotic calcite, and  $\beta = \frac{[Ca]_f}{[Ca]_0}$  is the fraction of original calcite remaining in the water (Bickle et al., 2015). The partition coefficient has been shown to vary with precipitation rates and temperature between  $\sim 0.02 - 0.2$  (Gabitov & Watson, 2006; Nehrke et al., 2007; Tesoriero & Pankow, 1996). We follow Bickle et al. (2015) and Emberson et al. (2018) and use a value of  $kd =$

0.05. Moreover, we neglect incorporation of Mg into calcite, because Mg incorporation into calcite at concentrations of  $\left[\frac{Mg^{2+}}{Ca^{2+}}\right] < 1$ , is expected to be <5% (Loste et al., 2003; Meldrum & Hyde, 2001). To estimate  $\beta$  (and thereby  $[Ca]_0$ ) we note that:

$$\frac{[Sr]_0}{[Ca]_0} = \frac{[Sr]_f}{[Ca]_f} \beta^{(1-kd)} \quad (13),$$

and because the concentration of sodium is unchanged:

$$[Na]_0 = [Na]_f \quad (14).$$

From equations (11) and (14) and the definition of  $\beta$ , we get:

$$\frac{1000 \times [Sr]_0}{[Ca]_0} = a + b \frac{[Na]_0}{[Ca]_0} = a + b \frac{[Na]_f}{[Ca]_f} \beta \quad (15).$$

Now, we have two estimates for  $\frac{[Sr]_0}{[Ca]_0}$  from equation (13) and (15), and we minimized the following equation numerically:

$$\frac{1000 \times [Sr]_f}{[Ca]_f} \beta^{1-kd} - a - b \frac{[Na]_0}{[Ca]_f} \beta = 0 \quad (16).$$

Uncertainties in the fraction of original calcite remaining in the water,  $\beta$ , were estimated from uncertainties in the regression parameters and the measured concentrations using a Monte Carlo routine. To this end, we repeated the minimization 10,000 times, randomly picking (1) the regression parameters from a bivariate normal distribution defined by the coefficients and variance-covariance matrix of the regression and (2)  $[Sr^{2+}]$ ,  $[Ca^{2+}]$ , and  $[Na^+]$  from the normal distribution defined by the measurement and uncertainty. We then estimated the uncertainty of  $\beta$  from the standard deviation of  $\beta$  from all Monte Carlo runs. The final uncertainty in the corrected calcium concentrations was estimated from this standard deviation and the analytical uncertainty of the original calcium measurement.

#### CO<sub>2</sub> budget from weathering reactions

We estimated the impact of erosion rates and the associated weathering patterns measured in Taiwan on the emission or drawdown of CO<sub>2</sub> by considering the balance of alkalinity and dissolved inorganic carbon (DIC) produced by weathering (see Table A.1 and equations A11 and A12 In Torres et al., 2016). The short-term effect of weathering on the inorganic CO<sub>2</sub> balance is:

$$[CO_2]_{st} = f_{sulf} 0.5 [Cat]_{carb}^{eq} + (1 - f_{sulf}) 0.5 [Cat]_{carb}^{eq} - (1 - f_{sulf}) ([Cat]_{carb}^{eq} + [Cat]_{sil}^{eq}) \quad (17),$$

where  $[CO_2]$  are the moles of CO<sub>2</sub> produced (positive  $[CO_2]$ ) or sequestered (negative  $[CO_2]$ ) per unit volume of weathering fluid. Noting that:

$$f_{sulf} = \frac{[SO_4]^{eq}}{[Cat]_{carb}^{eq} + [Cat]_{sil}^{eq}} \quad (18),$$

this equation can be simplified to:

$$[CO_2]_{st} = [SO_4]^{eq} - 0.5 [Cat]_{carb}^{eq} - [Cat]_{sil}^{eq} \quad (19).$$

Beyond the calcium carbonate compensation time (~10 ky; Zeebe & Westbroek, 2003), the production of alkalinity and dissolved cations by chemical weathering is balanced by the precipitation of (mostly) marine calcium carbonate. Then:

$$[CO_2]_{mt} = f_{sulf} 0.5 [Cat]_{carb}^{eq} + (1 - f_{sulf}) 0.5 [Cat]_{carb}^{eq} - 0.5 (1 - f_{sulf}) ([Cat]_{carb}^{eq} + [Cat]_{sil}^{eq}) \quad (20),$$

This equation can be simplified to:

$$[CO_2]_{mt} = [SO_4]^{eq} - 0.5 [Cat]_{sil}^{eq} \quad (21).$$

On multi-million year timescales, for a system under constant boundary conditions and a carbon cycle in steady state, the long-term inorganic CO<sub>2</sub> balance may depend only on the calcium produced by silicate weathering (Berner et al., 1983):

$$[CO_2]_{lt} = -0.5 [Ca]_{sil}^{eq} \quad (22).$$

where  $[Ca]_{sil}^{eq}$  is the equivalent calcium concentration from silicate weathering.

### Carbonate equilibria

The saturation state of calcium carbonate in water ( $\Omega_{cal}$ ) is defined as:

$$\Omega_{cal} = \frac{a_{Ca^{2+}} a_{CO_3^{2-}}}{K_{sp}} \quad (23),$$

where  $K_{sp}$  = is the equilibrium constant for the dissolution/precipitation reaction of calcium carbonate in water (Table 1). By definition, the second dissociation constant of carbonic acid ( $K_2$ ):

$$K_2 = \frac{a_{H^+} a_{CO_3^{2-}}}{a_{HCO_3^-}} \quad (24).$$

It follows that

$$\Omega_{cal} = \frac{K_2}{K_{sp}} \frac{a_{Ca^{2+}} a_{HCO_3^-}}{a_{H^+}} \quad (25).$$

In order to convert the measured concentrations into activities, we calculated the activity coefficients  $\gamma_i$  of for both calcium and bicarbonate using the Davies Equation (Davies, 1962):

$$\log_{10} \gamma_i = -A v_i^2 \left( \frac{\sqrt{I}}{1 + \sqrt{I}} - 0.3 I \right) \quad (26),$$

where  $A = 1.82 \times 10^6 (\epsilon T)^{-\frac{3}{2}}$  is an empirical constant,  $T$  is the temperature,  $\epsilon$  is the dielectric constant and  $I$  is the ionic strength of the solution given by:

$$I = \frac{1}{2} \sum_i v_i^2 [i] \quad (27).$$

We estimated the dielectric constant using an empirical fit to measurements of the dielectric constant at atmospheric pressures and temperatures between 273.15°K and 373.15°K (Table 4 in Archer & Wang, 1990)

$$\epsilon = 308.6464 e^{(-0.00459717 T)} \quad (28).$$

The overall temperature dependence of the factor  $A$  in equation 26 is small and  $A \approx 0.51$ . We also estimated the equilibrium constant for reaction  $j$  at water temperature  $T$  ( $K_{j,T}$ ) using the van't Hoff equation (van't Hoff, 1884):

$$\ln \left( \frac{K_{j,T}}{K_{j,298}} \right) = -\frac{\Delta H_j^\circ}{R} \left( \frac{1}{T} - \frac{1}{298.15} \right) \quad (29),$$

where  $K_{j,298}$  is the equilibrium constant of reaction  $j$  at 298.15 K,  $\Delta H_j^\circ$  is the standard enthalpy of reaction  $j$ , and  $R$  is the ideal gas constant. The saturation index for calcium carbonate in water  $SI_{cc}$  at temperature  $T$  is then

$$\begin{aligned} SI_{cal} &= \log_{10}(\Omega_{cal}) \\ &= \log_{10}(K_{2,T}) - \log_{10}(K_{sp,T}) \\ &\quad + \log_{10}(\gamma_{Ca^{2+}}[Ca^{2+}]) + \log_{10}(\gamma_{HCO_3^-}[HCO_3^-]) + pH \end{aligned} \quad (30).$$

In addition to the saturation index, we estimated the pH at equilibrium ( $pH_{eq}$ ) using:

$$pH_{eq} = \log_{10}(K_{sp,T}) - \log_{10}(K_{2,T}) - \log_{10}(\gamma_{Ca^{2+}}[Ca^{2+}]) - \log_{10}(\gamma_{HCO_3^-}[HCO_3^-]) \quad (31).$$

This  $pH_{eq}$  represents the pH of a solution that is exactly saturated with respect to the measured solutes. For all steps described above, uncertainties were propagated from the analytical uncertainties of measured concentrations. In these calculations, we only considered the contributions of solutes from weathering, cyclic sources, and the secondary carbonate lost to precipitation.

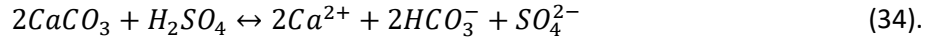
#### Estimate of pH change due to addition of sulphuric acid

We define  $pH_{SO_4}$  as the pH of a solution that results from the addition of sulphuric acid with concentration,  $[SO_4^{2-}]$ , to a calcium carbonate-buffered solution with an initial pH noted as  $pH_0$ : From equation (25), we recall that for a calcium carbonate-buffered solution at equilibrium (i.e. at  $\Omega_{cal}=1$ ) we have:

$$a_{H^+,0} = \frac{K_2}{K_{sp}} a_{Ca^{2+},0} a_{HCO_3^-,0} \quad (32),$$

$$a_{H^+,0} = \frac{K_2}{K_{sp}} \gamma_{Ca^{2+},0} [Ca^{2+}]_0 \gamma_{HCO_3^-,0} [HCO_3^-]_0 \quad (33),$$

where the subscript 0 denotes the quantities before the addition of sulphuric acid. We further assume that the following reaction of sulphuric acid with calcium carbonate dominates:



and that  $HCO_3^-$  remains the dominant dissolved carbonate species (which is reasonable for the range of pH between 6-8). After addition of the acid, the new activity of protons at equilibrium with the acid is:

$$\begin{aligned} a_{H^+,f} &= \frac{K_2}{K_{sp}} \gamma_{Ca^{2+},f} [Ca^{2+}]_f \gamma_{HCO_3^-,f} [HCO_3^-]_f \\ &= \frac{K_2}{K_{sp}} \gamma_{Ca^{2+},f} ([Ca^{2+}]_0 + 2[SO_4^{2-}]) \gamma_{HCO_3^-,f} ([HCO_3^-]_0 + 2[SO_4^{2-}]) \end{aligned} \quad (35).$$

where the subscript  $f$  denotes the final quantities after equilibration with the acid. Hence:

$$\begin{aligned} a_{H^+,f} &= \frac{K_2}{K_{sp}} \gamma_{Ca^{2+},f} \gamma_{HCO_3^-,f} ([Ca^{2+}]_0 [HCO_3^-]_0 + 2[SO_4^{2-}][Ca^{2+}]_0 + 2[SO_4^{2-}][HCO_3^-]_0 \\ &\quad + 4[SO_4^{2-}]^2) \end{aligned} \quad (36).$$

Next, we link the initial concentration of calcium,  $[Ca^{2+}]_0$ , and bicarbonate,  $[HCO_3^-]_0$ , to the initial pH,  $pH_0$  (or initial activity of protons  $a_{H^+,0}$ ). Let  $[CC]_0 = [Ca^{2+}]_0 [HCO_3^-]_0$ . Rearranging equation 33 we get:

$$[CC]_0 = [Ca^{2+}]_0 [HCO_3^-]_0 = \frac{K_{sp}}{K_2} \frac{a_{H^+,0}}{\gamma_{Ca^{2+},0} \gamma_{HCO_3^-,0}} \quad (37).$$

Further, we posit that we can express the concentration of calcium before the addition of sulphuric acid as a function of the concentration of bicarbonate and vice versa:



$$[Ca^{2+}]_0 = \frac{X_{Ca,0}}{2} [HCO_3^-]_0 \quad (38),$$

and

$$[HCO_3^-]_0 = \frac{2}{X_{Ca,0}} [Ca^{2+}]_0 \quad (39),$$

where  $X_{Ca,0}$  is the fraction of the total cation charge that is represented by calcium:

$$X_{Ca,0} = \frac{2[Ca^{2+}]_0}{\sum v_i [i]_0} \quad (40),$$

with

$$[Ca^{2+}]_0 = [Ca^{2+}]_f - 2[SO_4^{2-}] \quad (41),$$

and

$$\sum v_i [i]_0 = \sum v_i [i]_f - v_{Ca} 2[SO_4^{2-}] \quad (42).$$

Equations 38 - 42 allow us to express the concentrations of calcium and bicarbonate by their total concentration  $[CC]_0$

$$[Ca^{2+}]_0 = \sqrt{\frac{X_{Ca}}{2} [CC]_0} \quad (43),$$

and

$$[HCO_3^-]_0 = \sqrt{\frac{2}{X_{Ca}} [CC]_0} \quad (44).$$

Now, the combination of equations 36, 43, and 44 yields:

$$a_{H^+,f} = \frac{K_2}{K_{sp}} \gamma_{Ca^{2+},f} \gamma_{HCO_3^-,f} \left( [CC]_0 + 2[SO_4^{2-}] \sqrt{[CC]_0} \left( \sqrt{\frac{X_{Ca,0}}{2} + \frac{2}{X_{Ca,0}}} \right) + 4[SO_4^{2-}]^2 \right) \quad (45),$$

and the final pH after addition of sulphuric acid is:

$$pH_{SO_4} = -\log(a_{H^+,f}) \quad (46).$$

In our data analysis, we used equation 37 and an estimate of  $pH_0 = 8.47$  to calculate  $[CC]_0$ . Then, we calculated the pH change that is expected from  $pH_0$  due to the addition of sulphuric acid. We discarded 37 datapoints for which sulphate concentrations are larger than or within  $10 \mu\text{mol/L}$  of the calcium concentrations ( $[Ca^{2+}]_f - 2[SO_4^{2-}] < 10 \mu\text{mol/L}$ ). We define the initial pH,  $pH_0 = 8.47$ , as the unique value at which a regression through the data intersects the point  $pH_{SO_4} = pH_{eq} = pH_0$ . This point represents the necessity that the subsurface pH before addition of sulphuric acid is equal to the initial pH. All uncertainties were propagated from the analytical uncertainties of measured concentrations.

| Description                                       | Reaction  | Equilibrium constant at 298.15 °K | Standard enthalpy (kJ mol <sup>-1</sup> ) |
|---|---|-----------------------------------|---|
| Dissolution of $CO_2$ in water (Henry's constant) | $CO_{2(g)} \leftrightarrow CO_{2(aq)}$                | $K_H = 10^{-1.468}$               | $\Delta H_H^\circ = -19.98$               |
| First dissociation of $CO_2$ in water             | $CO_{2(aq)} + 2H_2O \leftrightarrow HCO_3^- + H_3O^+$ | $K_1 = 10^{-6.352}$               | $\Delta H_1^\circ = 9.109$                |
| Second dissociation of $CO_2$ in water            | $HCO_3^- + H_2O \leftrightarrow CO_3^{2-} + H_3O^+$   | $K_2 = 10^{-10.329}$              | $\Delta H_2^\circ = 14.90$                |
| Dissolution/Precipitation of carbonate in water   | $CaCO_3 \leftrightarrow Ca^{2+} + CO_3^{2-}$          | $K_{sp} = 10^{-8.480}$            | $\Delta H_{sp}^\circ = -9.612$            |

**Extended Data Table 1. Reactions, equilibrium constants and standard enthalpies.**

All parameters are from Parkhurst and Appelo (1999)

| Silicate  | Carbonate  |
|---|--|
| Global endmember compositions (Burke et al., 2018; Gaillardet et al., 1999) |  |
| $\left[\frac{Ca^{2+}}{Na^+}\right]_{sil} = 0.35 \pm 0.25$                   | $\left[\frac{Ca^{2+}}{Na^+}\right]_{carb} = 60 \pm 30$             |
| $\left[\frac{Mg^{2+}}{Na^+}\right]_{sil} = 0.25 \pm 0.20$                   | $\left[\frac{Mg^{2+}}{Na^+}\right]_{carb} = 30 \pm 15$             |
| Local endmember compositions: Forward model                                 |  |
| $\left[\frac{Ca^{2+}}{Na^+}\right]_{sil} = 0.10 \pm 0.06$                   | $\left[\frac{Ca^{2+}}{Na^+}\right]_{carb} = \infty$                |
| $\left[\frac{Mg^{2+}}{Na^+}\right]_{sil} = 0.80 \pm 0.59$                   | $\left[\frac{Mg^{2+}}{Na^+}\right]_{carb} = \infty$                |
| Local endmember compositions: Inverse model                                 |  |
| $\left[\frac{Na^+}{Ca^{2+}}\right]_{sil} = 10.9 \pm 4.7$                    | $\left[\frac{Na^+}{Ca^{2+}}\right]_{carb} = 0 \pm 0$               |
| $\left[\frac{Mg^{2+}}{Ca^{2+}}\right]_{sil} = 12.9 \pm 5.5$                 | $\left[\frac{Mg^{2+}}{Ca^{2+}}\right]_{carb} = 0.05 + 0.24 - 0.05$ |
| Seawater  | Hotsprings   |
| $\left[\frac{Na^+}{Ca^{2+}}\right]_{sw} = 45.5$                             | $\left[\frac{Na^+}{Ca^{2+}}\right]_{hs} = 315 \pm 150$             |
| $\left[\frac{Mg^{2+}}{Ca^{2+}}\right]_{sw} = 5.1$                           | $\left[\frac{Mg^{2+}}{Ca^{2+}}\right]_{hs} = 0.35 \pm 0.16$        |
| $\left[\frac{Cl^-}{Ca^{2+}}\right]_{sw} = 53$                               | $\left[\frac{Cl^-}{Ca^{2+}}\right]_{hs} = 5.4 \pm 2.4$             |
| $\left[\frac{SO_4^{2-}}{Ca^{2+}}\right]_{sw} = 11.0$                        | $\left[\frac{SO_4^{2-}}{Ca^{2+}}\right]_{hs} = 1.7 \pm 0.8$        |
| $\left[\frac{K^+}{Ca^{2+}}\right]_{sw} = 1.0$                               | $\left[\frac{K^+}{Ca^{2+}}\right]_{hs} = 1.4 \pm 0.6$              |

**Table 2. Endmember compositions**

#### 4. File description

The data consists of a single Excel spreadsheet with 5 tabs. In addition, all data tables are provided as tab-delimited text version:

- Tab 1 – Data-S1\_Raw-water-chemistry (measurements)
- Tab 2 – Data-S2\_10Be-Erosion-Rates (compiled cosmogenic nuclide erosion rate data)
- Tab 3 – Data-S3\_Hotspring-Data (Public hotspring data from the study area)
- Tab 4 – Data-S4\_Suspended-sediment-data (from-Emberson et al, 2018)
- Tab 5 – Data-S5\_Derived-quantities

## 5. Acknowledgement

This project has received funding from the European Union's Horizon 2020 research and innovation programme under the Marie Skłodowska-Curie grant agreement No 841663.

## 6. References

- Archer, D. G. & Wang, P. (1990). The dielectric constant of water and Debye-Hückel limiting law slopes. *J. Phys. Chem. Ref. Data* 19, 371-41, <https://doi.org/10.1063/1.555853>
- Berner, R. A., Lasaga, A. C. & Garrels, R. M. (1983). The carbonate-silicate geochemical cycle and its effect on atmospheric carbon dioxide over the past 100 million years. *Am. J. Sci.* 283, 641-683, <https://web.colby.edu/ch217public/files/2016/02/Berner-Lasaga-and-Garrels-1983.pdf>
- Bickle, M. J., Tipper, E., Galy, A., Chapman, H. & Harris, N. (2015). On discrimination between carbonate and silicate inputs to Himalayan rivers. *Am. J. Sci.* 315, 120-166, <https://doi.org/10.2475/02.2015.02>
- Bufe, A., Hovius, N., Emberson, R., Rugenstein, J. K. C., Galy, A., Hassenruck-Gudipati, H. J., & Chang, J.-M. (2021). Co-variation of silicate, carbonate and sulfide weathering drives CO<sub>2</sub> release with erosion. *Nature Geoscience*, 14(4), 211–216, <https://doi.org/10.1038/s41561-021-00714-3>
- Burke, A., Present, T. M., Paris, G., Rae, E. C. M., Sandilands, B. H., Gaillardet, J., Peucker-Ehrenbrink, B., Fischer, W. W., McClelland, J. W., Spencer, R. G. M., Voss, B. M., & Adkins, J. F. (2018). Sulfur isotopes in rivers: Insights into global weathering budgets, pyrite oxidation, and the modern sulfur cycle. *Earth Planet. Sc. Lett.* 496, 168-177, <https://doi.org/10.1016/j.epsl.2018.05.022>
- Chen, C., Willett, S. D., West, A. J., Dadson, S., Hovius, N., Christl, M., & Shyu, J. B. H. (2020). The impact of storm-triggered landslides on sediment dynamics and catchment-wide denudation rates in the southern Central Range of Taiwan following the extreme rainfall event of Typhoon Morakot. *Earth Surf. Proc. Land.* 45, 548-564, <https://doi.org/10.1002/esp.4753>
- Davies, C. W. Ion association. (Butterworths, 1962).
- Emberson, R., Galy, A., & Hovius, N. (2018). Weathering of Reactive Mineral Phases in Landslides Acts as a Source of Carbon Dioxide in Mountain Belts. *Journal of Geophysical Research: Earth Surface*, 123(10), 2695–2713, <https://doi.org/10.1029/2018jf004672>
- Fellin, M. G., Chen, C.-Y., Willett, S. D., Christl, M. & Chen, Y.-G. (2017). Erosion rates across space and timescales from a multi-proxy study of rivers of eastern Taiwan. *Global Planet. Change* 157, 174-193, <https://doi.org/j.gloablacha.2017.07.012>
- Gabitov, R. I. & Watson, E. B. (2006). Partitioning of strontium between calcite and fluid. *Geochem. Geophys.* 7, <https://doi.org/10.1029/2005GC001216>
- Gaillardet, J., Dupré, B., Louvat, P. & Allègre, C. J. (1999). Global silicate weathering and CO<sub>2</sub> consumption rates deduced from the chemistry of large rivers. *Chem. Geol.* 159, 3-30, [https://doi.org/10.1016/S0009-2541\(99\)00031-5](https://doi.org/10.1016/S0009-2541(99)00031-5)
- Loste, E., Wilson, R. M., Seshadri, R. & Meldrum, F. C. (2003). The role of magnesium in stabilising amorphous calcium carbonate and controlling calcite morphologies. *J. Cryst. Growth* 254, 206-218, [https://doi.org/10.1016/S0022-0248\(03\)01153-9](https://doi.org/10.1016/S0022-0248(03)01153-9)
- Meldrum, F. C. & Hyde, S. T. (2001). Morphological influence of magnesium and organic additives on the precipitation of calcite. *J. Cryst. Growth* 231, 544-558, [https://doi.org/10.1016/S0022-0248\(01\)01519-6](https://doi.org/10.1016/S0022-0248(01)01519-6)
- Moon, S., Chamberlain, C. P. & Hilley, G. E. (2014). New estimates of silicate weathering rates and their uncertainties in global rivers. *Geochim. Cosmochim. Ac.* 134, 257-274, <https://doi.org/10.1016/j.gca.2014.02.033>

- Nehrke, G., Reichart, G. J., Van Cappellen, P., Meile, C. & Bijma, J. (2007). Dependence of calcite growth rate and Sr partitioning on solution stoichiometry: Non-Kossel crystal growth. *Geochim. Cosmochim. Ac.* 71, 2240-2249, <https://doi.org/10.1016/j.gca.2007.02.002>
- Parkhurst, D. L. & Appelo, C. User's guide to PHREEQC (Version 2)(1999). A computer program for speciation, batch-reaction, one-dimensional transport, and inverse geochemical calculations. Water-resources investigations report 99-4529, <https://doi.org/10.3133/wri994259>
- Schwanghart, W. & Scherler, D. (2014). Short Communication: TopoToolbox 2 – MATLAB-based software for topographic analysis and modeling in Earth surface sciences. *Earth Surf. Dynam.* 2, 1-7, <https://doi.org/10.5194/esurf-2-1-2014>
- Tesoriero, A. J. & Pankow, J. F. (1996). Solid solution partitioning of Sr<sup>2+</sup>, Ba<sup>2+</sup>, and Cd<sup>2+</sup> to calcite. *Geochim. Cosmochim. Ac.* 60, 1053-1063, [https://doi.org/10.1016/0016-7037\(95\)00449-1](https://doi.org/10.1016/0016-7037(95)00449-1)
- Torres, M. A., West, A. J., Clark, K. E., Paris, G., Bouchez, J., Ponton, C., Feakins, S. J., Galy, V., & Adkins, J. F. (2016). The acid and alkalinity budgets of weathering in the Andes–Amazon system: Insights into the erosional control of global biogeochemical cycles. *Earth Planet. Sc. Lett.* 450, 381-391, <https://doi.org/10.1016/j.epsl.2016.06.012>
- van't Hoff, M. J. H. *Etudes de dynamique chimique.* (Frederik Muller & Company, 1884).
- West, A. J., Galy, A. & Bickle, M. (2005). Tectonic and climatic controls on silicate weathering. *Earth Planet. Sc. Lett.* 235, 211-228, <https://doi.org/10.1016/j.epsl.2005.03.020>
- Zeebe, R. E. & Westbroek, P. (2003). A simple model for the CaCO<sub>3</sub> saturation state of the ocean: The “Strangelove,” the “Neritan,” and the “Cretan” Ocean. *Geochem. Geophys.* 4, <https://doi.org/10.1029/2003GC000538>